THE JOURNAL OF BIOLOGICAL CHEMISTRY VOL. 291, NO. 44, pp. 22881–22893, October 28, 2016
© 2016 by The American Society for Biochemistry and Molecular Biology, Inc. Published in the U.S.A.

A Novel Role of Chromodomain Protein CBX8 in DNA Damage Response*

Received for publication, March 5, 2016, and in revised form, July 22, 2016 Published, JBC Papers in Press, August 23, 2016, DOI 10.1074/jbc.M116.725879

Jay Oza[‡§¶‖1], **Bratati Ganguly**[¶1], **Atul Kulkarni**[¶], **Vasudeva Ginjala**[¶], **Ming Yao**[¶], **and Shridar Ganesan**[§¶2]

From the [‡]*MD-PhD Program, Rutgers–Robert Wood Johnson Medical School, New Brunswick, New Jersey 08903, the* [§]*Department of Cellular and Molecular Pharmacology, Rutgers–Graduate School of Biomedical Sciences, Piscataway, New Jersey 08854, the* [¶]*Rutgers Cancer Institute of New Jersey, New Brunswick, New Jersey 08903, and the* [‖]*Dartmouth Hitchcock Medical Center, Lebanon, New Hampshire 03766*

Induction of DNA damage induces a dynamic repair process involving DNA repair factors and epigenetic regulators. Chromatin alterations must occur for DNA repair factors to gain access to DNA lesions and restore original chromatin configuration to preserve the gene expression profile. We characterize the novel role of CBX8, a chromodomain-containing protein with established roles in epigenetic regulation in DNA damage response. CBX8 protein rapidly accumulates at the sites of DNA damage within 30 s and progresses to accumulate until 4 min before gradually dispersing back to its predamage distribution by 15 min. CBX8 recruitment to the sites of DNA damage is dependent upon PARP1 activation and not dependent on ATM activation. CBX8 biochemically interacts with TRIM33, and its recruitment to DNA damage is also dependent on the presence of TRIM33. Knockdown of CBX8 using siRNA significantly reduces the efficiency of both homologous and the other nonhomologous recombination, as well as increases sensitivity of cells to ionizing radiation. These findings demonstrate that CBX8 functions in the PARP-dependent DNA damage response partly through interaction with TRIM33 and is required for efficient DNA repair.

DNA damage response is characterized by rapid activation of a signal transduction cascade, resulting in the recruitment of DNA repair machinery and chromatin remodeling complexes to the sites of DNA damage (1–3). Signals for recruiting and activating these downstream targets are transduced by means of phosphorylation, ubiquitination, sumoylation, and poly-(ADP-ribosyl)ation, as well as a multitude of various other post-translational modifications (4–6). For instance, upon sensing DNA double-stranded breaks, Mre11-Rad50-Nbs1 (MRN) complexes facilitate the ATM auto-phosphorylation and activation (4). ATM then activates downstream mediators and effectors such as pH2AX and CHK1. Likewise, upon sensing multiple DNA breaks, poly(ADP-ribose)polymerase (PARP)[3] is activated and auto-poly(ADP-ribosyl)ates itself along with a variety of downstream substrates such as histones (7).

PARP are a family of enzymes (8) with a variety of critical cellular roles including those in DNA repair, transcriptional regulation, and metabolic function (9–12). Recent observations that cells deficient in homologous recombination (HR) mediated repair are sensitive to PARP inhibitors suggests an important role of PARP in DNA repair (13, 14). The known function of PARP in single-strand break repair is thought to be central to its "synthetic lethality" with BRCA1/2 loss (15). However, PARP has a broader role in DNA repair and is active at single strand breaks, stalled replication forks, and DNA double-stranded breaks. Moreover, the exact functional role of PARP in DNA repair pathways remains unclear. Recent data suggest the poly(ADP-ribose) polymers (PARs) induced by PARP activity at DNA breaks can recruit chromatin remodeling enzymes such as ALC1 (amplified in liver cancer 1), and they may be critical for proper repair (16–18). However, little is known about such downstream effects of PARP activity.

Recent studies have identified the role of polycomb group proteins such as Bmi1 in DNA damage response (19). Polycomb genes are thought to mediate transcriptional silencing and have been implicated in the control of embryogenesis, development, stem cell self-renewal, and heritable epigenetic states, as well as cell proliferation and cancer (1, 4, 20–27). Polycomb group proteins can be classified based on the complexes they form. There are two main complexes: polycomb repressive complex 1 (PRC1) and polycomb repressive complex 2 (PRC2). PRC2 functions to initiate chromatin silencing by virtue of its various histone methyltransferase activities (among others), whereas PRC1 functions to maintain the silent state by binding methylated histones and recruiting more PRC2 complexes, thereby spreading the inactivation signal (22, 28–31).

Chromobox proteins (CBX), named so for the presence of chromodomain, are a component of PRC1 complex (32). CBX proteins have been found to be recruited to sites of DNA damage in the setting of a large screen (33). This study described the localization of several polycomb-group proteins and NuRD complex to sites of DNA breaks. We now further characterize

* This work was supported by Fellowship 808057 from the New Jersey State Commission on Cancer Research (to J. O.), Department of Defense Breast Cancer Research Program Award W81XWH-10-BCRP-PREDOC (to J. O.), and funding from the NCI, National Institutes of Health, the Val Skinner Foundation, Hugs for Brady Foundation and the Triple Negative Breast Cancer Foundation (to S. G.). The authors declare that they have no conflicts of interest with the contents of this article. The content is solely the responsibility of the authors and does not necessarily represent the official views of the National Institutes of Health.

[1] Both authors contributed equally to this work.

[2] To whom correspondence should be addressed. E-mail: ganesash@cinj.rutgers.edu.

[3] The abbreviations used are: PARP, poly(ADP-ribose) polymerase; HR, homologous recombination; PAR, poly(ADP-ribose) polymer; PRC, polycomb repressive complex; IF, immunofluorescence; IdU, 5-iodo-2′-deoxyuridine; IP, immunoprecipitation; MEF, mouse embryonic fibroblast; DZNep, 3-deazaneplanocin A-HCl; [W], Western blotting.

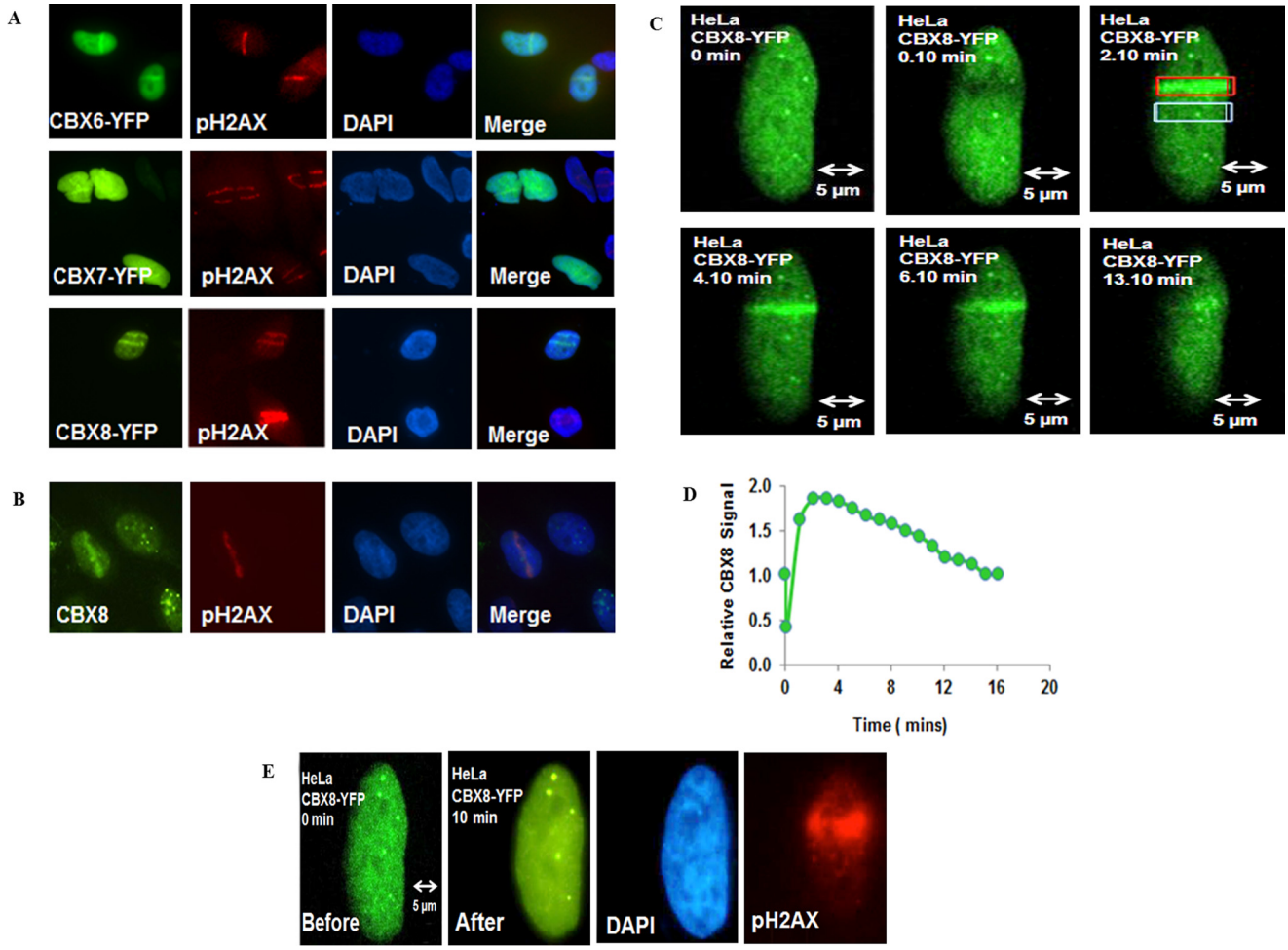

FIGURE 1. **CBX proteins are recruited to the sites of DNA damage.** *A*, HeLa cells were plated in a 4-well chamber slide, transfected with CBX6-YFP, CBX7-YFP, or CBX8-YFP and treated with IdU. DNA was subsequently damaged using UV laser microirradiation. The cells were fixed immediately after inducing DNA damage and stained for pH2AX. *B*, U2OS cells were subjected to UV laser microirradiation and fixed within 10 min of DNA damage. The cells were stained for endogenous CBX8 and pH2AX and visualized using a fluorescence microscope (40×) magnification. *C*, HeLa cells were plated as in *A* and under similar experimental condition; DNA was damaged using the UV laser (500 iterations in a narrow rectangular region) of Zeiss LSM 510 Meta confocal microscope at 63× water immersion. The images were captured right before and after damage and subsequently at 1-min intervals. *D*, the pixel intensity in the rectangular box surrounding the DNA damage was measured using ImageJ. Normalized pixel intensity in the region of damage compared with the undamaged region, called the "relative CBX8 signal," was plotted as a function of time. *E*, the slide was fixed after the time lapse experiment and stained with pH2AX antibody, and the cell on which the live cell imaging was performed was found and verified for the presence of pH2AX staining in the region of damage.

the role of CBX8 in the DNA damage response. Polycomb group proteins play a critical role in regulation of histone modifications, and our data suggest that they may be involved downstream of PARP activation in DNA repair processes.

Results

Polycomb Group Proteins Are Recruited to the Sites of DNA Damage—We investigated the recruitment of CBX proteins to the sites of DNA damage. YFP fusion constructs of CBX6, CBX7, and CBX8 were expressed in cells and localization to sites of UV laser scissors-induced DNA breaks was monitored by immunofluorescence (IF). The cells were fixed 2 min after induction of breaks and processed for IF staining for pH2AX to identify regions of induced DNA breaks. Our results (Fig. 1, *A* and *B*) indicate that CBX6, CBX7, and CBX8, which exhibit exclusive nuclear localization under normal conditions, are rapidly co-localized with pH2AX at the sites of DNA damage. CBX6 and CBX8 exhibited the strongest localization, whereas CBX7 exhibited a rather modest recruitment to the sites of DNA damage. Under identical experimental conditions CBX2-YFP or CBX4-YFP did not demonstrate a significant recruitment to the sites of DNA damage (results not shown). Furthermore, we note that the observed recruitment of CBX6, CBX7, and CBX8 was both rapid and transient, with recruitment being seen minutes after induction of DNA damage and declining after 10–15 min. Of all the CBX proteins studied, CBX8 recruitment appeared to be the strongest, and hence we decided to study its role at the DNA damage sites in more detail. We confirmed the recruitment of endogenous CBX8 to laser scissors-induced DNA breaks by performing IF using antibodies to CBX8 and pH2AX (Fig. 1*B*).

Time Course of CBX8 Recruitment to Break Site—To characterize the time course of CBX8 recruitment, we performed live cell confocal imaging of cells transfected with CBX8-YFP and incubated with 5-iodo-2′-deoxyuridine (IdU) (34) overnight, using line scan feature of UV laser to induce local DNA breaks (Zeiss LSM 510 Meta). When we systematically imaged at 1-min intervals, we found that CBX8 appeared at the sites of

DNA breaks almost immediately after the damage (within 1 min of the break). The highest abundance of CBX8 at DNA breaks was in 2–4 min and resolved back to its predamage distribution by 15 min (Fig. 1, *C* and *D*). We confirmed the presence of DNA damage under the experimental conditions used for live cell imaging by fixing the cells after the experiment and staining for pH2AX (Fig. 1*E*).

Structure-Function Analysis of the CBX8 Recruitment—CBX8 is known to have a well conserved N-terminal chromodomain, as well as the C-terminal repressor box. In addition, a recent comparative sequence analysis between the various vertebrate polycomb homologs has identified novel motifs in CBX8 (35), including two "AT hook-like" motifs similar to the DNA-binding AT hook motif, a signature Cx8.1 motif specific to CBX8 in the various vertebrate species analyzed, as well as Arg- and Glu-rich RED motif (Fig. 2*A*). There is also a stretch of ~150 amino acids near the C terminus without any annotation but has been shown to bind MLL fusion partner AF9 (36). We call this domain ABD (for AF9 binding domain). We also investigated domains that are required for the recruitment of CBX8 to the sites of DNA damage by generating a set of deletion constructs lacking one or multiple of these motifs both from the N and C terminus of the protein into pEGFP-N3 (Fig. 2*A*). Expression of GFP fusion constructs was verified by Western blotting (Fig. 2*B*). We then performed our live cell imaging experiments with these deletion constructs (Fig. 2*C*) and found that the N-terminal chromodomain is essential for localization to DNA breaks, because constructs that lack this domain fail to localize to DNA breaks. However, the chromodomain is not by itself sufficient for CBX8 recruitment. The inclusion of the adjacent ATHL1 motif (CBX8(1–2)-GFP) enables a weak localization to the sites of DNA damage. When the next motif, Cx8.1, was also included in our construct (CBX8(1–3)-GFP), we saw a localization signal that was similar to that of the full length of CBX8 (CBX8(WT)-GFP). These results suggest that the chromodomain, ATHL1, and Cx8.1 motifs contribute to the localization of CBX8 to the sites of DNA damage. Together, these findings suggest that the N-terminal chromodomain, ATHL1, and the Cx8.1 form a minimal unit that is essential and sufficient for CBX8 recruitment to the sites of DNA damage. The findings of these structure-function data are summarized in Fig. 2*D*.

To reaffirm that the recruitment of CBX8-GFP to the sites of UV laser-induced DNA damage is specific and restricted to the damage site, we performed our experiments using either GFP alone or H2B-GFP plasmids. We found that neither of these proteins was enriched at the sites of DNA damage (results not shown).

CBX8 Recruitment Is Independent of Other PRC Components—Because the results of our structure-function analysis suggested that chromodomain is important for CBX8 recruitment to the sites of DNA damage and chromodomain is known to interact with H3K27me3, we further investigated whether inhibiting EZH2, known as a histone methyltransferase that methylates H3K27, would abrogate CBX8 localization. We found that CBX8 localization to the sites of DNA damage persisted despite treating cells with an EZH2 inhibitor, DZNep (Fig. 3*A*) (37), at concentrations that significantly reduce the levels of H3K27me3 (Fig. 3*B*). Similar results were obtained using another specific inhibitor of PRC2 (GSK 126) (38) (Fig. 3, *C* and *D*). These findings suggest that binding of chromodomain to methylated histones may be dispensible for recruitment of CBX8 to sites of DNA breaks. CBX8 has been reported to interact with other polycomb group proteins such as Bmi1 (39). To investigate whether CBX8 recruitment is driven by Bmi1, we tested CBX8 recruitment in $Bmi1^{-/-}$ MEFs ($INK4a^{-/-}$, $ARF^{-/-}$ background) and found that CBX8 localization in both WT MEFs and $Bmi1^{-/-}$ MEFs is identical; thus CBX8 recruitment is independent of Bmi1 (Fig. 3*E*).

CBX8 Recruitment Is Independent of ATM and ATR—UV microirradiation in the setting of IdU pretreatment is known to induce DNA double-strand breaks and other DNA lesions that are known to activate ATM and ATR kinase pathways (40). To investigate the role of ATM and/or ATR activation on CBX8 recruitment to DNA breaks, we performed live cell imaging experiment on cells treated with DMSO or ATM inhibitor (KU-0055933) and ATR inhibitor (VE-821). We found that treatment with ATM or ATR inhibitor (41) had no effect on the recruitment of CBX8 to the sites of DNA damage (Fig. 3, *F* and *G*).

CBX8 Recruitment Is Dependent on PARP Pathway—Given the extremely rapid dynamics by which CBX8 is recruited to the sites of DNA damage, which is similar to the dynamics of PARP activation, we investigated the role of PARP in this process (42, 43). We found that treatment with a PARP1 inhibitor (KU-0058948), at doses that abolish auto-poly(ADP-ribosyl)ation of PARP1, abolished CBX8 recruitment to the DNA damage sites (Fig. 4, *A* and *B*). Moreover, CBX8 showed no recruitment to DNA breaks in $Parp1^{-/-}$ MEFs, confirming that PARP activity is required for this process (Fig. 4, *C* and *D*).

CBX8 Recruitment Is Dependent on TRIM33—Recent investigations have identified that PARP activation at DNA breaks leads to recruitment of several proteins, including ALC1, a chromatin remodeling protein, and TRIM33, a transcriptional repressor and ubiquitin ligase (18, 44–47). We found that CBX8 recruitment was intact in cells harboring shRNA-mediated knockdown of ALC1 (Fig. 4, *E* and *F*), suggesting that CBX8 is recruited to DNA breaks independently of ALC1. We investigated CBX8 recruitment in cells transfected with TRIM33 specific shRNA and found that CBX8 localization to the sites of DNA damage was absent in cells with TRIM33 knockdown compared with control shRNA-treated cells (Fig. 4, *G* and *H*). This suggests that CBX8 recruitment to DNA breaks is dependent upon TRIM33.

CBX8 Interacts with TRIM33—To determine whether there is a biochemical interaction between CBX8 and TRIM33, we performed co-immunoprecipitation (co-IP) experiments. We transfected HEK293 cells with a plasmid expressing FLAG-HA-tagged CBX8 (pOZ-FH-C-CBX8) or control plasmid (p-OZ-FH-C). These cells were then exposed to UV radiation, and samples were harvested at various time points after DNA damage. The nuclear extracts were co-immunoprecipitated using anti-FLAG affinity beads and analyzed by Western blotting. We found that FLAG-CBX8 co-immunoprecipitates TRIM33 (Fig. 4*I*). The result suggests that CBX8 interacts with TRIM33. These interactions are present both at

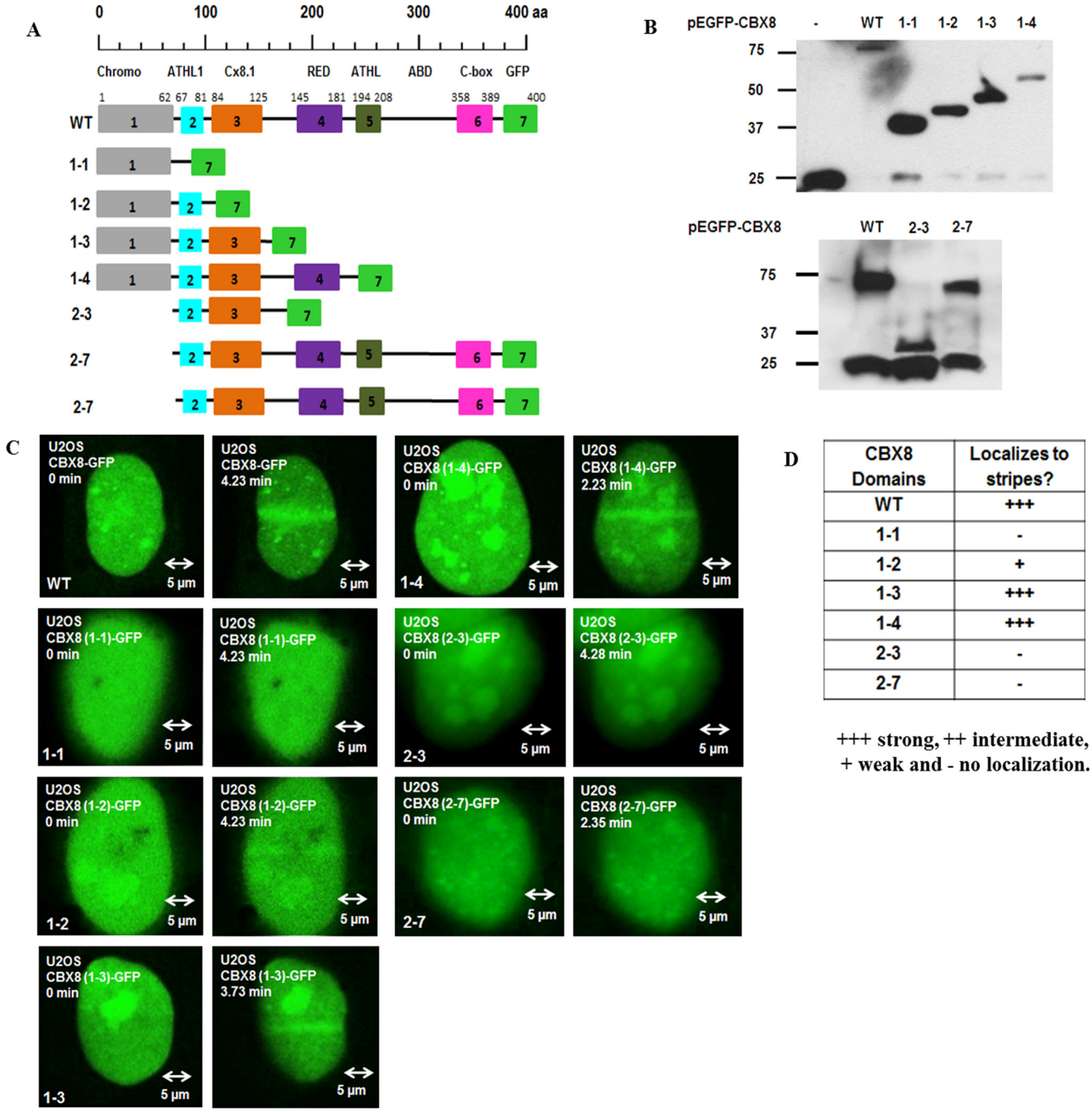

D

CBX8 Domains	Localizes to stripes?
WT	+++
1-1	-
1-2	+
1-3	+++
1-4	+++
2-3	-
2-7	-

+++ strong, ++ intermediate, + weak and - no localization.

FIGURE 2. **Structure-function analysis of the CBX8 domains responsible for its recruitment to sites of DNA damage.** *A*, the domain architecture of CBX8 is indicated above the WT construct. The various deletion segments of CBX8 were cloned into pEGFP-N3 vector as indicated. The *numbers* below the WT construct indicate the amino acid span of each domain. The *numbers* below the deletion constructs indicate the range of amino acids cloned for that particular construct. Constructs are drawn to scale. *B*, U2OS cells were transfected with the different CBX8-GFP deletion constructs. Protein expression is shown in Western blot stained with anti-GFP antibody. The *minus sign* indicates transfection with empty vector expressing GFP alone. WT CBX8-GFP is ~70 kDa and the 25 kDa is the GFP band. *C*, U2OS cells were transfected with the CBX8-GFP deletion constructs and treated with IdU. DNA damage was performed the following day using the UV laser of Zeiss LSM 510 Meta confocal microscope, and live cell imaging was performed as described earlier. Images taken prior to induction of DNA damage and a representative time point during interval of peak localization noted for WT-CBX8 (from 2 to 10 min) are shown for each construct. *D*, summary of the structure-function data.

baseline and after induction of DNA damage, suggesting that they are constitutive interactions independent of presence of DNA breaks.

Knockdown of CBX8 Reduces the Frequency of the Homologous and Non-homologous Recombination and Increases Radiosensitivity—We further investigated the functional role of CBX8 in homologous and non-homologous mediated DNA repair using a specific reporter assays (48–50). We found that the knockdown of CBX8 by using two separate CBX8-specific siRNAs (siCBX8–1 and -2) significantly reduced the efficacy of both HR- and NHEJ-mediated repair using separate specific GFP-based reporter systems (Fig. 5, *A–D*). These data strongly suggest that CBX8 is required for efficient HR-mediated as well as NHEJ-mediated DNA repair.

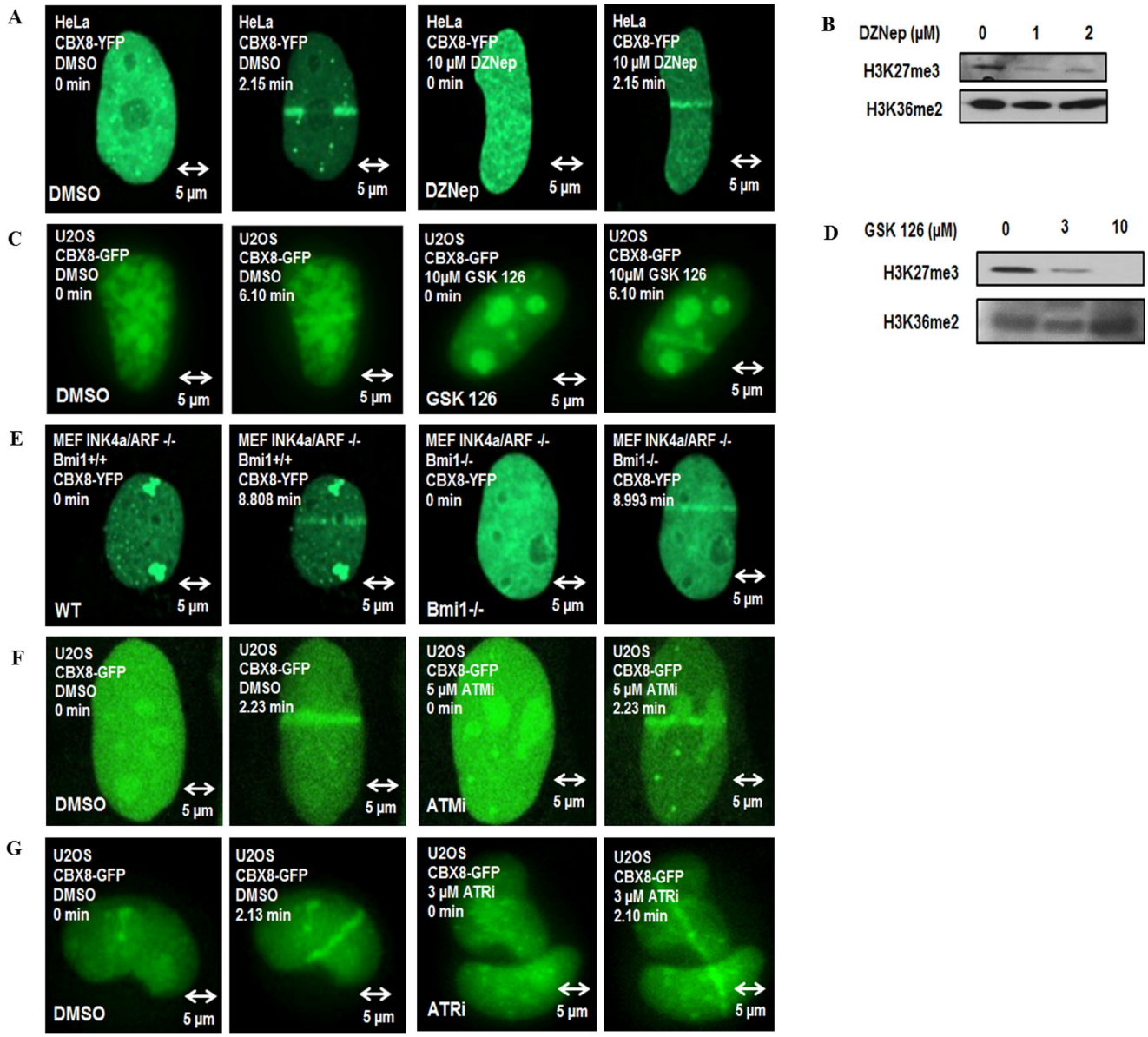

FIGURE 3. **CBX8 recruitment is independent of other PRC components and PI3-like kinase pathway.** *A*, HeLa cells were plated onto a glass-bottomed chamber slide and transfected with CBX8-YFP. The cells were treated overnight with IdU, as well as either DMSO or 10 μM DZNep. DNA was damaged using Zeiss LSM 510 Meta confocal microscope, and time lapse imaging was performed. *B*, Western blot demonstrating the efficacy of DZNep compound in reducing the levels of H3K27me3, the primary product of EZH2, while not affecting the levels of H3K36 dimethylation. *C*, U2OS cells were plated onto a glass-bottomed chamber slide and transfected with CBX8-GFP. The cells were treated overnight with IdU, as well as either DMSO or 10 μM GSK 126. *D*, Western blot demonstrating the effect of GSK 126 treatment on level of H3K27me3; H3K36 dimethylation was used as control. *E*, MEFs (INK4a$^{-/-}$, ARF$^{-/-}$ background) with either WT (Bmi1$^{+/+}$) or deficient (Bmi1$^{-/-}$) Bmi1 were plated onto glass-bottomed chamber slides and transfected with CBX8-YFP. The cells were treated overnight with IdU. Live cell imaging experiments were performed as described previously. *F*, U2OS cells were plated onto a glass-bottomed chamber slide and transfected with CBX8-GFP. The cells were treated overnight with IdU, as well as either DMSO or 5 μM ATM inhibitor (KU-0055933). DNA was damaged using Zeiss LSM 510 Meta confocal microscope, and time lapse imaging was performed. *G*, U2OS cells were plated onto a glass-bottomed chamber slide, transfected with CBX8-GFPP, treated with 3 μM ATR inhibitor (VE-821) or control, and subjected to laser scissors and GFP visualized as above.

We next investigated the role of knockdown of CBX8 on the sensitivity to ionizing radiation. We found that the knockdown of CBX8 significantly reduces the ability of U2OS cells to form colonies following exposure to ionizing radiation (Fig. 5, *E–G*) (3). These results suggest that CBX8 plays an important functional role in promoting efficient DNA repair as well as cell survival following DNA damage.

Discussion

DNA breaks lead to rapid activation of PARP1/2, catalyzing the assembly of new PAR chains onto chromatin. Loading of nascent PAR modifications onto chromatin leads to the recruitment of several chromatin remodeling enzymes, including ALC1 and ubiquitin ligases such as TRIM33, which contributes to dynamic local chromatin relaxation and allows for efficient repair (18, 47, 51). Here, we demonstrate that the polycomb factor, CBX8, plays a role in PARP-dependent DNA damage repair pathway. We confirm that CBX8 is rapidly recruited to sites of DNA breaks in a PARP-dependent fashion (33). We further demonstrate that CBX8 also plays a role in efficient repair of DNA lesions because knockdown of CBX8 leads to decrease in efficacy of both HR and NHEJ, as well as increased

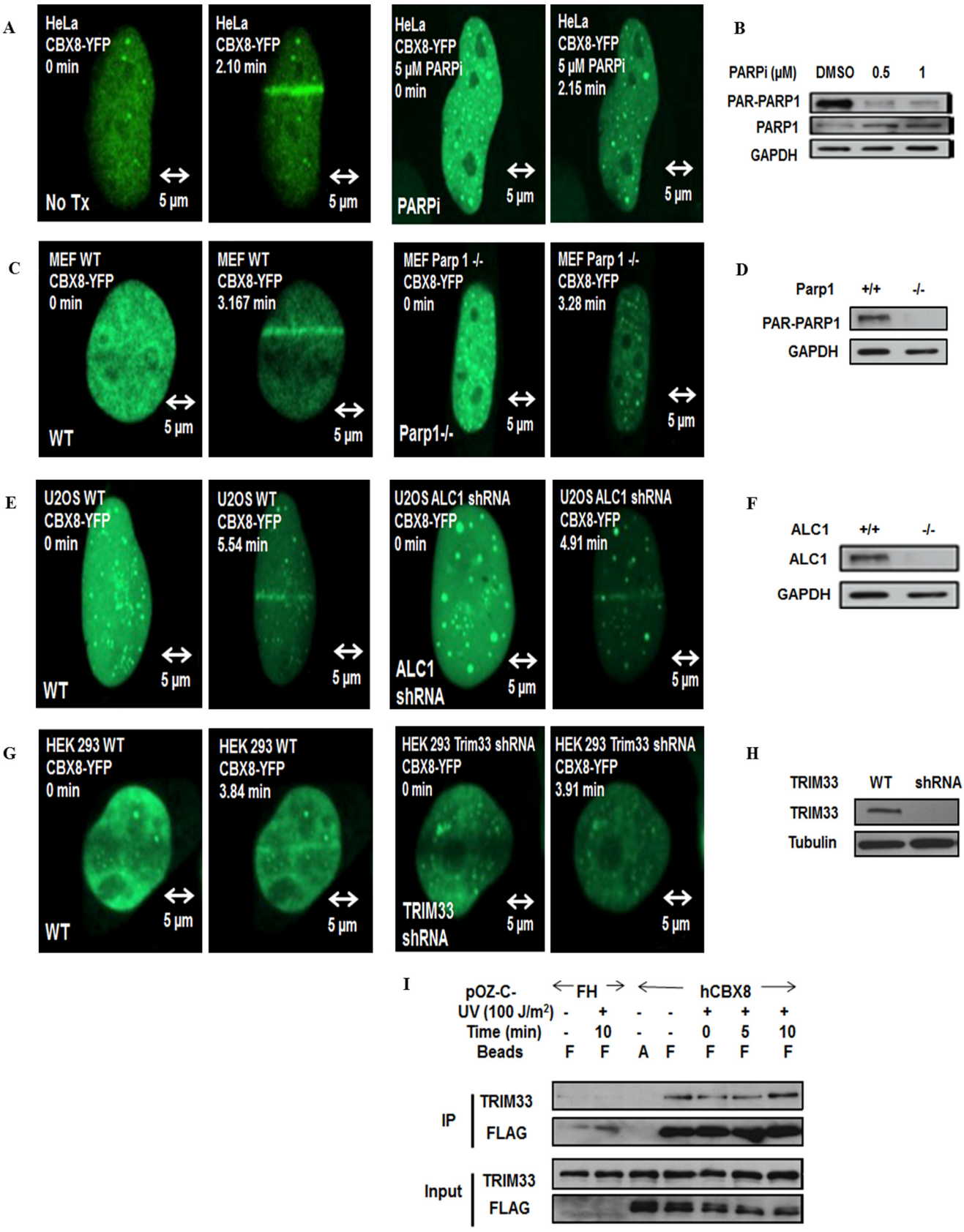
A
HeLa CBX8-YFP 0 min
No Tx
5 μm
HeLa CBX8-YFP 2.10 min
5 μm
HeLa CBX8-YFP 5 μM PARPi 0 min
PARPi
5 μm
HeLa CBX8-YFP 5 μM PARPi 2.15 min
5 μm
B
PARPi (μM) DMSO 0.5 1
PAR-PARP1
PARP1
GAPDH
C
MEF WT CBX8-YFP 0 min
WT
5 μm
MEF WT CBX8-YFP 3.167 min
5 μm
MEF Parp 1 -/- CBX8-YFP 0 min
Parp1-/-
5 μm
MEF Parp 1 -/- CBX8-YFP 3.28 min
5 μm
D
Parp1 +/+ -/-
PAR-PARP1
GAPDH
E
U2OS WT CBX8-YFP 0 min
WT
5 μm
U2OS WT CBX8-YFP 5.54 min
5 μm
U2OS ALC1 shRNA CBX8-YFP 0 min
ALC1 shRNA
5 μm
U2OS ALC1 shRNA CBX8-YFP 4.91 min
5 μm
F
ALC1 +/+ -/-
ALC1
GAPDH
G
HEK 293 WT CBX8-YFP 0 min
WT
5 μm
HEK 293 WT CBX8-YFP 3.84 min
5 μm
HEK 293 Trim33 shRNA CBX8-YFP 0 min
TRIM33 shRNA
5 μm
HEK 293 Trim33 shRNA CBX8-YFP 3.91 min
5 μm
H
TRIM33 WT shRNA
TRIM33
Tubulin
I
pOZ-C- ← FH → ← hCBX8 →
UV (100 J/m²) - + - - + + +
Time (min) - 10 - - 0 5 10
Beads F F A F F F F
IP
TRIM33
FLAG
Input
TRIM33
FLAG

radiosensitivity (3). These data suggest that a loss of CBX8 has a general effect on efficacy of DNA double-stranded break repair. This observation raises the possibility that CBX8 may play an early role in process of DNA breaks that is required for both HR and NHEJ.

CBX8 is part of PRC1, which includes both Bmi1 and RING1a/b, and CBX8 has been shown to interact with Bmi1 (39). Interestingly, Bmi1 has also been reported to play a role in DNA damage repair and is also recruited to sites of laser scissors-induced local DNA breaks (19, 52, 53). However, Bmi1 has very different dynamics of recruitment to damage site from CBX8. Bmi1 is recruited to sites of laser scissor-induced DNA breaks within minutes. However, unlike CBX8, which is present at breaks only for 15–20 min, Bmi1 is retained at these sites for several hours. Bmi1 recruitment and prolonged retention is also dependent on ATM activation, whereas CBX8 recruitment is completely dependent upon PARP activation and is unaffected by ATM or ATR inhibition. These observations suggest that the function of CBX8 in DNA repair may be independent of that of Bmi1. Consistent with this hypothesis, the recruitment of CBX8 to sites of DNA breaks in not impaired in Bmi1$^{-/-}$; INK4a$^{-/-}$ MEFs. Thus Bmi1 and CBX8, although present in the same PRC1 complex in the setting of epigenetic regulation, may have independent roles in DNA repair. It is known that the conserved N-terminal chromodomain region of CBX8 binds methylated histones (54). Our studies show that the chromodomain of CBX8 is required but not sufficient for its recruitment to DNA breaks. The adjacent AT-hook like domain (ATHL1) and CBX8 signature motif Cx8.1 are also required for efficient recruitment to DNA breaks. The functional roles of ATHL1 and Cx8.1 motifs are at present unclear. It has been hypothesized that the presence of DNA binding domain adjacent to the histone binding chromodomain in CBX proteins might lead to a three-way CBX-histone-DNA interaction that can restrict nucleosome dynamics (35). Our results demonstrate that CBX8 recruitment to the sites of DNA damage may not require the presence of histone H3 methylated at Lys^{27} (H3K27me3). Reduction of global H3K27me3 levels by DZNep or GSK 126 did not eliminate localization of CBX8 to laser scissors-induced DNA breaks. This again suggests that the chromodomain of CBX8 may be binding to other methylated substrates in the context of DNA damage. Several studies have suggested that CBX8 chromodomain may have different substrate specificities than other polycomb chromodomains and may include non-histone peptides as potential binding targets (55–57).

CBX8 is required for efficient DNA repair because knockdown of CBX8 leads to both reduced efficiency of HR and NHEJ, as well as increased radiosensitivity. This phenotype is very similar to that seen with knockdown of another PARP-dependent DNA repair factor, TRIM33. Indeed CBX8 biochemically interacts with TRIM33, as seen by endogenous co-immunoprecipitation, and the localization of CBX8 to sites of DNA breaks is dependent upon the presence of TRIM33. This suggests a functional interaction between CBX8 and TRIM33 in the DNA repair process.

Of note, CBX8 appears to be dependent upon TRIM33 expression, but not on ALC1, for its recruitment to DNA breaks, even though the localization of TRIM33 is dependent on ALC1 localization (47). One possible explanation is that with ALC1 knockdown, although TRIM33 localization is greatly diminished, enough TRIM33 is present to support CBX8 localization. Alternatively, it may be that CBX8 localization depends on some activity of TRIM33 that does not require TRIM33 localization at DNA breaks. Interestingly, unlike the interaction of TRIM33 with ALC1, which is only present after induction of DNA damage (47), the biochemical interaction of TRIM33 with CBX8 appears to be constitutive (Fig. 4*I*). Thus TRIM33 and CBX8 may biochemically interact even in absence of DNA damage, when TRIM33 is not localized at DNA breaks. This constitutive interaction with TRIM33 may be required for proper localization of CBX8 to DNA breaks, even in the absence of efficient recruitment of TRIM33 to DNA breaks. This finding suggests that CBX8 and TRIM33 may also be functionally related independent of the presence of DNA damage.

Interestingly, both CBX8 and TRIM33 have been reported to function in transcriptional silencing, suggesting that these proteins may be involved in local transcriptional silencing at sites of DNA damage. ATM activation has been shown to induce local chromatin silencing as part of the DNA damage response (58). Because TRIM33 and CBX8 appear to be more associated with PARP activation than ATM/ATR activation, it is tempting to speculate that these proteins may partly function to induce transcriptional silencing downstream of PARP activation during the DNA damage response. Because PARP activation may lead to increased chromatin access, active transcriptional silencing may be required to prevent the inappropriate transcriptional activation near DNA breaks. Understanding the process by which DNA damage is repaired in this setting requires further investigation.

Materials and Methods

Tissue Culture and Cell Lines—The cells were cultured in DMEM (Gibco 11995) supplemented with 10% FBS (GeneMate S-1200-500) and 1% antibiotics (either 100 units/ml penicillin + 100 μg/ml streptomycin (Gibco 15140) or 1× antibiotic-

FIGURE 4. **Proteins responsible for the recruitment of CBX8 to the sites of DNA breaks.** *A*, CBX8-YFP localization was imaged after DNA damage in HeLa cells either untreated or treated with 5 μM PARPi (KU-0058948). *B*, HeLa cells treated with various concentrations of PARP inhibitor (KU-0058948) were harvested in NETN buffer and analyzed for Western blotting using antibody recognizing PAR, with bands showing PARylated PARP1, PARP1 itself, and GAPDH. *C*, CBX8-YFP localization was imaged after DNA damage in WT or Parp1$^{-/-}$ MEFs. *D*, whole cell extracts of WT or Parp1$^{-/-}$ MEFs were prepared using NETN buffer and analyzed by Western blotting for auto-poly(ADP-ribosyl)ation of PARP1 (PAR-PARP1) and GAPDH. *E*, CBX8-YFP localization was imaged after DNA damage in WT or ALC1 shRNA U2OS cells. *F*, whole cell extracts of WT or ALC1 shRNA U2OS cells were prepared and analyzed by Western blotting for ALC1 and GAPDH. *G*, CBX8-YFP localization was imaged after DNA damage in WT or TRIM33 shRNA-treated U2OS cells. *H*, whole cell extracts of WT or TRIM33 shRNA-treated U2OS cells were prepared using NETN buffer and analyzed by Western blotting for TRIM33 and GAPDH. *I*, HEK293 cells were transfected with FLAG-HA (pOZ-C-FH) or hCBX8-FLAG-HA (pOZ-C-hCBX8-FH) plasmid, treated with indicated dose of UV radiation, and harvested at various time points. Nuclear extracts were incubated with anti-FLAG (*F*) or protein A beads (*A*). Immunoprecipitated samples were analyzed by Western blotting for the presence of TRIM33 and FLAG. *Input* represents 5% of the sample loaded for IP reaction.

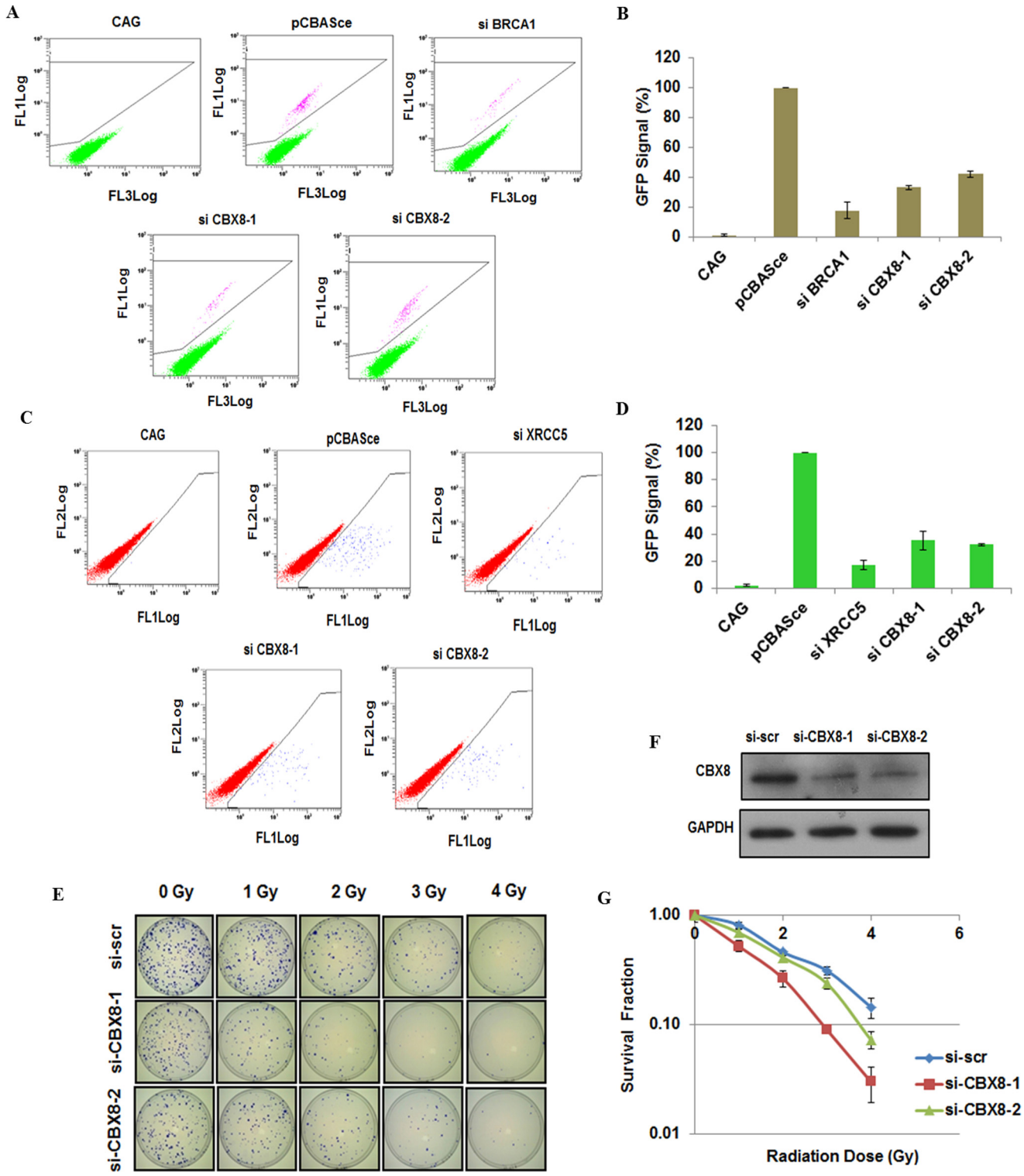

FIGURE 5. **Knockdown of CBX8 decreases the frequency of HR/NHEJ and sensitizes U2OS cells to ionizing radiation.** *A*, DR-U2OS cells with a stably integrated tandem GFP reporter for HR were treated with pCBASce (plasmid bearing I-SceI endonuclease) or CAG (control plasmid), along with scrambled siRNA or two different siRNAs targeting CBX8. The percentage of GFP-positive cells (indicative of the cells having undergone successful DNA repair by homologous recombination) was measured by flow cytometry. GFP-positive cells (plotted in FL1) were gated with representative experiment shown. Results from a representative experiment are shown. *B*, results of HR assay from five independent experiments are plotted. The *error bars* indicate ± S.D. *C*, U2OS EJ5-GFP reporter cells were used to measure the efficiency of NHEJ in this setting. GFP-positive cells (plotted in FL1) were gated with representative experiment shown. *D*, results of NHEJ assay from three independent experiments are plotted. The *error bars* indicate ± S.D. *E*, U2OS cells were transfected with the appropriate siRNAs and plated into 10-cm plates (1000 cells/plate) ($n = 3$). The cells were treated with the indicated doses of γ-radiation and incubated for 3 weeks, and their ability to form colonies was assayed by crystal violet staining. A representative 10-cm plate from a set of triplicate is shown. *F*, siRNA-treated cells were plated in a 6-well plate in parallel to the 10-cm dishes used for colony forming assay. The samples were harvested 72 h after siRNA treatment and assayed for CBX8 levels. *G*, graphical representation of the colony counts.

antimycotic (Gibco 15240)). The cells were washed with Dulbecco's PBS (Gibco 14190) prior to trypsinization (Gibco 25200) and maintained in a humidified incubator with 5% CO_2. Bmi1 control (INK4a$^{-/-}$, ARF$^{-/-}$, Bmi1$^{+/+}$) and deficient (INK4a$^{-/-}$, ARF$^{-/-}$, Bmi1$^{-/-}$) MEFs were obtained from Maarten van Lohuizen (Netherlands Cancer Institute). Parp1$^{-/-}$ MEFs were obtained from Kathleen Scotto (Rutgers Cancer Institute of New Jersey). ALC1-deficient U2OS cells were obtained from Simon Boulton (18). They were cultured in 2 μg/ml puromycin.

Plasmid and siRNA Transfection—CBX6, CBX7, and CBX8 fused with YFP and cloned into pCMVFlag were obtained from Tom Kerppola (59). CBX8-GFP and its deletion constructs were cloned into pEGFP-N3 as described below. All plasmids were transfected using Opti-MEM I-reduced serum medium (Gibco 31985). For transfection in a 6-well plate, 2×10^5 cells were plated/well in DMEM. The following day, the medium was changed to Opti-MEM I prior to transfection. The cells were then transfected using 1 μg of the desired plasmid (diluted in 250 μl Opti-MEM I) and 4 μl of Lipofectamine 2000 (Invitrogen 11668-019) (diluted in 250 μl of Opti-MEM I) using manufacturer's protocol. The medium was changed back to DMEM 4–6 h post-transfection. For transfection into 4-well chamber slides, 1×10^5 cells were plated/well and transfected using 0.5 μg of plasmid and 1.5 μl Lipofectamine 2000 (each diluted in 30 μl of Opti-MEM I). siRNA targeting CBX8 was obtained from Sigma (si-CBX8: SASI_Hs01_00047550: CUCGCUUGCUCGCAGCCUU, custom designed for si-UTR (si-UTR: 5′-GCGUGAGCUUGGCAUAGUG-3′). Negative control siRNA was also obtained from Sigma (si-scr: SIC001–5 × 1NMOL: proprietary sequence). For transfection in a 6-well plate, the cells were plated as described before and transfected using 50 pmol of siRNA, unless otherwise stated (diluted in 250 μl of Opti-MEM I), and 5 μl Lipofectamine 2000 according to manufacturer's protocol. The medium was changed back to DMEM 24 h post-transfection. In a 2-ml final volume, this siRNA concentration corresponds to 25 nM.

Preparation of Cell Extracts—To prepare whole cell extracts, culture medium from plate was aspirated on ice. The cells were washed twice with ice-cold PBS. The cells were then scraped in 250 μl of NETN buffer (20 mM Tris, pH 8.0, 150 mM NaCl, 1 mM EDTA, 0.5% Nonidet P-40, 1× Protease inhibitor; Roche 04693124001) and incubated on ice for 15 min. Samples were sonicated using Branson Sonifier 450 (duty cycle, 10%; output control, 3) three times for six pulses each. This sonication protocol gave very consistent and reproducible results, and thus whole cell extracts were collected by centrifugation at 14,000 rpm for 10 min at 4 °C. The samples were quantitated using Bio-Rad protein reagent (Bio-Rad 500-0006) on the Beckman Coulter DU640 model spectrophotometer.

SDS-PAGE and Western Blotting—Protein samples were mixed 1:1 with 2× Laemmli sample buffer (Sigma S3401-1VL) and boiled for 10 min at 95 °C. The 10-μg sample/well was loaded on a 10% Tris-glycine SDS-polyacrylamide gel. The kaleidoscope protein ladder (Bio-Rad 161-0375) was used for molecular weight standard. The gels were run at 100 V for ~1 h and transferred onto a PVDF membrane (Bio-Rad 162-0177) at 15 V for 1 h using Trans-Blot S.D. semi-dry transfer cell (Bio-Rad 170-3940). The membrane was then blocked for 1 h at room temperature with 5% nonfat dry milk (Bio-Rad 170-6404) prepared in PBST (PBS + 1% Tween 20). The blot was then incubated with the desired dilution of primary antibody overnight at 4 °C and washed four times (15 min each) with PBST. This was followed by incubation with the desired dilution of secondary antibody in PBST for 1 h at room temperature. The blot was washed again with PBST and probed with a Western blot detection kit (Millipore 64-202BP).

Co-immunoprecipitation—To perform co-IP experiments, 2×10^6 HEK293 cells were plated per 10-cm plate. The following day, the cells were transfected with 8 μg of pOZ-FH-C or pOZ-CBX8-FH-C plasmid (cloned as described later) and 40 μl of Lipofectamine 2000 (each in 1.5 ml of Opti-MEM I). The medium was changed 4–6 h after transfection. 48–72 h after transfection, UV damage (100 J/m^2) was performed by administering 254 nm UVC radiation using UV Stratalinker 1800 (Stratagene). At the desired time points, the nuclear extracts were harvested and co-IP was performed using the nuclear complex co-IP kit (Active Motif 54001) as per the manufacturer's instructions. Briefly, the cells were washed extensively with ice-cold PBS (supplemented with phosphatase inhibitors). The cells were scraped and harvested in PBS (supplemented with phosphatase inhibitors) and centrifuged at 1500 rpm for 5 min, 4 °C. The pellet was resuspended in 1× hypotonic buffer and incubated on ice for 15 min. The cells were disrupted by addition of detergent and gentle pipetting. The suspension was then centrifuged at 14,000 × *g* for 30 s, 4 °C. Supernatant (cytoplasmic fraction) was discarded, and the pellet (nuclear fraction) was resuspended in complete digestion buffer followed by the addition of enzymatic shearing mixture. After brief vortex, suspension was incubated for 90 min at 4 °C. The shearing reaction was stopped by 0.5 M EDTA. Samples were centrifuged at 14,000 × *g* for 10 min, 4 °C. The supernatant (nuclear extract) was quantitated as described earlier. For co-IP, 300 μg of nuclear extract was diluted to 500 μl in high stringency IP incubation buffer (supplemented with detergent and NaCl for further stringency). The samples were precleared using protein A-agarose beads (Upstate 16-156) and incubated with 60 μl of prewashed anti-FLAG M2 affinity gel (Sigma A2220) or protein A-agarose beads overnight at 4 °C. The following day beads were washed three times with high stringency IP wash buffer (supplemented with BSA) and then three times with high stringency IP wash buffer (without BSA). Co-IP complex were eluted with 1:1 mixture of 2× Laemmli buffer and high stringency IP wash buffer and boiled for 10 min at 95 °C. The eluted samples were subsequently used for SDS-PAGE analysis.

Assay for Homologous and Non-homologous Recombination—HR assay (47, 48, 60) was performed by plating 2×10^5 DR-U2OS cells, whereas NHEJ assay was performed by plating U2OS EJ5-GFP cells (50) per well in a 6-well plate. The following day, the cells were transfected with 50 pmol of siRNA. 48 h after transfection of siRNA, the cells were transfected with the I-SceI endonuclease bearing plasmid pCBASce or the control plasmid along with a second smaller dose of siRNA (25 pmol). 72–96 h after transfection with the endonuclease, the cells were harvested for flow cytometry. Briefly, the cells were washed with PBS, trypsinized, and washed again with PBS. The cells

TABLE 1
List of the primers used for Cloning CBX8

Primer	Sequence (5′ → 3′)	Strand
pOZ-FH-C 1F	GATGAAGATCTTTGAACCATGGAGCTTTCAGCGGTG	Sense
pOZ-FH-C 7R	CCGCTCGAGTCTTTTCTCTTTAAAAAAGCC	Anti-sense
pEGFP-N3 1F	AGATCTCGAGCGTGAACCATGGAGCTTTCAGCGGTG	Sense
pEGFP-N3 2F	AGATCTCGAGCGTGAACCATGGAGCTCTATGGCCCCAAAAAG	Sense
pEGFP-N3 1R	ATTCGAAGCTTGCTCTCTTTCCCTTTCCTC	Anti-sense
pEGFP-N3 2R	ATTCGAAGCTTGTTTGAGGAGGAAGGTTTTGGG	Anti-sense
pEGFP-N3 3R	ATTCGAAGCTTGGTTTCGAAGGCCCTCCCGGGC	Anti-sense
pEGFP-N3 4R	ATTCGAAGCTTGATCCACTCTGCTGGTACC	Anti-sense
pEGFP-N3 7R	ATTCGAAGCTTGTCTTTTCTCTTTAAAAAAGCC	Anti-sense

were resuspended in PBS supplemented with 5% FBS. The percentage of cells positive for GFP was measured by using Cytomics FC500 series flow cytometer (Beckman Coulter).

Colony Forming Assay—Colony forming assay was performed (61) wherein 2×10^5 U2OS cells were plated per well in a 6-well plate. The following day, the cells were transfected with siRNA as described earlier. Twenty-four hours post-transfection, the cells were trypsinized and plated into 10 cm plates (1000 cells/plate) in triplicates. Simultaneously, an aliquot of cells were also plated in a 6-well plate for protein knockdown analysis by Western blotting. 48 h post-transfection, the cells were irradiated with 10 grays of ionizing radiation administered from a Cesium-137 source from Gammacell 40 Exactor (Best Theratronics). 2–3 weeks post-transfection, the cells were visualized under a light microscope for the formation of visible colonies. When the colonies reached a size of greater than 50 cells/colony, the cells were washed with PBS, fixed, and stained simultaneously with methanol + 0.5% crystal violet for 15 min. The plates were destained and washed with a few changes of fresh water until the background was clear. After allowing the plates to dry at room temperature, the colonies were counted, and the plates were photographed on a light table using iPhone 3GS (Apple).

RNA Extraction and cDNA Synthesis—RNA was extracted from a confluent 6-well plate using the TRIzol reagent (Invitrogen 15596-026) as per manufacturer's instructions. Briefly, the cells were washed with PBS followed by lysis using 1 ml of TRIzol reagent. The homogenized samples were incubated for 5 min at room temperature. This was followed by addition of 0.2 ml of chloroform and vigorous shaking of the tubes for 15 s. The samples were then incubated for 3 min at room temperature. Samples were centrifuged at 12,000 × *g* for 15 min at 4 °C. The upper aqueous phase containing the RNA was transferred into a fresh tube followed by precipitation using 0.5 ml of isopropanol. Samples were incubated for 10 min at room temperature and centrifuged at 12,000 × *g* for 10 min at 4 °C. The RNA pellet was washed once with 75% ethanol and centrifuged at 7500 × *g* for 5 min at 4 °C. The RNA pellet was air dried followed by resuspension in RNase-free water and incubated for 10 min at 55 °C to dissolve it. This RNA was then purified using RNeasy mini kit (Qiagen 74104) along with the on-column DNase digestion (Qiagen 79254) according to the manufacturer's protocol. The column purified RNA was quantitated using NanoDrop 1000 (Thermo Scientific) and used for subsequent cDNA synthesis. cDNA was synthesized using SuperScript III first strand synthesis system (Invitrogen 18080-051) according to the manufacturer's instructions using 1 μg of total RNA and oligo$(dT)_{20}$ primer provided with the kit.

Plasmid Construction—cDNA from HeLa was used to PCR amplify CBX8 using a 2× PCR master mix (Roche 11 636 103 001) and primers (purchased from Sigma). DNA from the CBX8-specific band was excised from the gel and purified using the QIAquick gel extraction kit (Qiagen 28704). CBX8 inserts, as well as the parent plasmids: pOZ-FH-C (62) and pEGFP-N3 (Clontech 6080-1), were restriction digested using the appropriate restriction enzymes (New England Biolabs: BglII R0144S, HindIII R0104S, XhoI R0146S). The restricted products were again gel-purified and subsequently used for ligation using the T4 DNA ligase (New England Biolabs M0202S). Ligations were performed using ~3:1 molar ratio of insert: plasmid at 16 °C for 60 min, followed by inactivation at 65 °C for 10 min. Following ligation, the samples were transformed into subcloning efficiency DH5α competent cells (Invitrogen 18265-017) using the supplied protocol and plated onto selective LB-Agar plates (ampicillin 100 μg/ml or kanamycin 30 μg/ml) and incubated overnight at 37 °C. Surviving colonies were analyzed for the presence of insert by colony-PCR using a pair of insert specific primers. Plasmids from positive colonies were harvested by growing the leftover colonies in 200 ml of selective medium overnight followed by maxi-prep using HiSpeed plasmid maxi kit (Qiagen 12663). The purified plasmids were also verified by sequencing using the sequencing primers (Tables 1 and 2).

UV Laser Induction of DNA Damage—The cells were plated onto a 4-well Lab-Tek chamber slides (NUNC 177399) for the UV laser scissors experiments. If needed, the cells were transfected the following day with the desired GFP/YFP fusion plasmid. 4–6 h post-transfection medium was replaced with DMEM supplemented with 10 μM IdU (Sigma I7125). UV laser treatment was performed the following day. The chamber slides were mounted on the stage of Zeiss Axiovert 200M integrated with PALM microlaser work station. Narrow linear regions within nuclei were marked for UV laser irradiation using PALM robo v3.2 software. UVA radiation (30 Hz, 337 nm) was delivered in the demarcated regions using a 40× objective. The cells were either fixed immediately or returned to the incubator and fixed at the desired time point followed by immunocytochemical staining.

Live Cell Imaging and Quantitation—Live cell imaging experiments were performed by plating cells on a Lab-Tek chambered cover glass (NUNC 155383). The following day, the cells were transfected with GFP/YFP fusion plasmid. Fresh medium supplemented with IdU was added 4–6 h after transfection. The next day, a live cell imaging experiment was performed using the Zeiss LSM 510 Meta laser scanning confocal microscope. The cells were visualized using 63× water immersion objective. DNA within a narrow rectangular region in the

TABLE 2
List of the primers used for sequencing CBX8

Primer	Sequence (5′ → 3′)	Strand
CBX8 internal	CCTTCGAAACATGGGTTTGT	Sense
pOZ-FH-C upstream	CCCTCAAAGTAGACGGCATC	Sense
pOZ-FH-C downstream	TTGTGTCTCCCGGATCTCTC	Anti-sense
pEGFP-N3 upstream	CGTGTACGGTGGGAGGTCTA	Sense
pEGFP-N3 downstream	GCTGAACTTGTGGCCGTTTA	Anti-sense

nucleus was damaged using 500 iterations of the fast line scan with UV (351/364 nm) laser operated at 75% of maximum output. Images were acquired immediately before the DNA damage, immediately after DNA damage, and periodically thereafter using the argon laser (488 nm). Quantitation was performed using ImageJ. The mean pixel intensity in the rectangular box surrounding the DNA damage was measured using ImageJ. This mean pixel intensity was then normalized for differences in expression level, microscope gain, and focus drifts by dividing with the mean pixel intensity of a box of the same size from other adjacent undamaged region in the nucleus. This ratio, called the "relative CBX8 signal," was plotted as a function of time.

Immunocytochemistry—The cells were washed with PBS and fixed with 4% paraformaldehyde for 10 min at room temperature. The cells were permeabilized using 0.5% Triton X-100 (10 min, room temperature), washed with PBS, and then incubated with primary antibodies in 5% normal goat serum (Vector Laboratories H-1200). After washing, the cells were incubated with secondary antibodies in 5% normal goat serum and washed again. Finally, the cells were mounted using mounting medium containing DAPI (Vector Laboratories S-1000). All of the solutions were made in PBS that was used in the experiment. The slides were visualized, and the images were captured using either Nikon Eclipse 80i or Zeiss Axiovert 200M fluorescence microscopes.

Drugs and Antibodies—EZH2 inhibitor (DZNep) was obtained from Victor E. Marquez (NCI, National Institutes of Health) (37). EZH2 inhibitor (GSK 126) was obtained from MedChem Express®. ATM kinase inhibitor (KU-0055933) and PARP inhibitor (KU-0058948) were obtained from KuDOS Pharmaceuticals (Cambridge, UK). ATR inhibitor (VE-821) was obtained from Cayman Chemicals. Rabbit polyclonal anti-CBX8 antibody was a kind gift of Tom Kerppola (59) (used at a dilution of 1:100 for IF and 1:2000 for Western blotting [W]). Alternatively, rabbit polyclonal anti-CBX8 from Abcam (ab70796) was also used (1:2000 [W]). Mouse monoclonal anti-pH2AX was from Millipore (clone JBW301, 05-636, 1:250 [IF], 1:2000 [W]). Mouse monoclonal anti-PAR polymer was from Trevigen (clone 10HA, 4335-MC-100-AC, 1:1000 [W]). Rabbit monoclonal anti-PARP1 was from Cell Signaling (clone 46D11, 9532, 1:1000 [W]). Mouse monoclonal anti-GAPDH was from Abcam (clone 6C5, ab8245, 1:10000 [W]). Mouse monoclonal anti-ALC1 was from Abcam (clone 2170C3a, ab51324, 1:500 [W]). Rabbit polyclonal anti-FLAG was from Sigma (F7425, 1:1000 [W]). Mouse monoclonal anti-GFP was from Clontech (clone JL-8, 632380, 1:2000 [W]). Rabbit polyclonal anti-H3K27me3 was from Millipore (07-449, 1:100 [IF], 1:2000 [W]). Rabbit polyclonal anti-TRIM33 was from Bethyl Labs (A301-060A, 1:1000 [W]). Mouse monoclonal anti-Tubulin was from Sigma (clone B-5-1-2, T5168, 1:10000 [W]). Rabbit polyclonal anti-H2A (total) was obtained from Millipore (07–146, 1:8000 [W]). The following HRP-conjugated secondary antibodies were used for Western blotting at 1:1000 dilution: goat anti-mouse IgG (Millipore, 12-349) or goat anti-rabbit IgG (Millipore, 12-348). The secondary antibodies used (1:250 dilution) for immunofluorescence were from the Jackson ImmunoResearch Laboratories: FITC goat anti-rabbit IgG (111-095-144), TRITC-goat anti-rabbit IgG (111-025-144), FITC-goat anti-mouse IgG (115-095-166), or TRITC goat anti-mouse IgG (115-025-166).

Author Contributions—J. O., A. K., V. G., and S. G. conceived the study. J. O. and B. G. designed, performed, and analyzed the experiments. J. O., B. G., and S. G. wrote the first draft of the manuscript. J. O. and B. G. contributed to the preparation of the figures. J. O., B. G., A. K., V. G., M. Y., and S. G. made critical revisions and approved the final version. All authors reviewed and approved of the final manuscript.

Acknowledgments—We thank Victor E. Marquez (NCI, National Institutes of Health) for gifting DZNep and Tom K. Kerppola for sharing various CBX-YFP plasmid constructs.

References

1. Hoeijmakers, J. H. (2009) DNA damage, aging, and cancer. *N. Engl. J. Med.* **361,** 1475–1485
2. Ciccia, A., and Elledge, S. J. (2010) The DNA damage response: making it safe to play with knives. *Mol. Cell* **40,** 179–204
3. Xiao, W., Ou, C., Qin, J., Xing, F., Sun, Y., Li, Z., and Qiu, J. (2014) CBX8, a novel DNA repair protein, promotes tumorigenesis in human esophageal carcinoma. *Int. J. Clin. Exp. Pathol.* **7,** 4817–4826
4. Jackson, S. P., and Bartek, J. (2009) The DNA-damage response in human biology and disease. *Nature* **461,** 1071–1078
5. van Attikum, H., and Gasser, S. M. (2009) Crosstalk between histone modifications during the DNA damage response. *Trends Cell Biol.* **19,** 207–217
6. Lukas, J., Lukas, C., and Bartek, J. (2011) More than just a focus: the chromatin response to DNA damage and its role in genome integrity maintenance. *Nat Cell Biol.* **13,** 1161–1169
7. Lafon-Hughes, L., Di Tomaso, M. V., Méndez-Acuña, L., and Martínez-López, W. (2008) Chromatin-remodelling mechanisms in cancer. *Mutat. Res.* **658,** 191–214
8. Quénet, D., El Ramy, R., Schreiber, V., and Dantzer, F. (2009) The role of poly(ADP-ribosyl)ation in epigenetic events. *Int. J.. Biochem. Cell Biol.* **41,** 60–65
9. Huertas, D., Sendra, R., and Muñoz, P. (2009) Chromatin dynamics coupled to DNA repair. *Epigenetics* **4,** 31–42
10. Sinha, M., and Peterson, C. L. (2009) Chromatin dynamics during repair of chromosomal DNA double-strand breaks. *Epigenomics* **1,** 371–385
11. Chi, P., Allis, C. D., and Wang, G. G. (2010) Covalent histone modifications: miswritten, misinterpreted and mis-erased in human cancers. *Nat. Rev. Cancer* **10,** 457–469
12. Xu, Y., and Price, B. D. (2011) Chromatin dynamics and the repair of DNA double strand breaks. *Cell Cycle* **10,** 261–267
13. D'Amours, D., Desnoyers, S., D'Silva, I., and Poirier, G. G. (1999) Poly(ADP-ribosyl)ation reactions in the regulation of nuclear functions. *Biochem. J.* **342,** 249–268
14. Ganguly, B., Dolfi, S. C., Rodriguez-Rodriguez, L., Ganesan, S., and Hirshfield, K. M. (2016) Role of biomarkers in the development of PARP inhibitors. *Biomark Cancer* **8,** 15–25
15. Dedes, K. J., Wilkerson, P. M., Wetterskog, D., Weigelt, B., Ashworth, A., and Reis-Filho, J. S. (2011) Synthetic lethality of PARP inhibition in cancers lacking BRCA1 and BRCA2 mutations. *Cell Cycle* **10,** 1192–1199

16. Ahel, I., Ahel, D., Matsusaka, T., Clark, A. J., Pines, J., Boulton, S. J., and West, S. C. (2008) Poly(ADP-ribose)-binding zinc finger motifs in DNA repair/checkpoint proteins. *Nature* **451,** 81–85
17. Gagné, J. P., Isabelle, M., Lo, K. S., Bourassa, S., Hendzel, M. J., Dawson, V. L., Dawson, T. M., and Poirier, G. G. (2008) Proteome-wide identification of poly(ADPribose) binding proteins and poly(ADP-ribose)-associated protein complexes. *Nucleic Acids Res.* **36,** 6959–6976
18. Ahel, D., Horejsí, Z., Wiechens, N., Polo, S. E., Garcia-Wilson, E., Ahel, I., Flynn, H., Skehel, M., West, S. C., Jackson, S. P., Owen-Hughes, T., and Boulton, S. J. (2009) Poly(ADP-ribose)-dependent regulation of DNA repair by the chromatin remodeling enzyme ALC1. *Science* **325,** 1240–1243
19. Ginjala, V., Nacerddine, K., Kulkarni, A., Oza, J., Hill, S. J., Yao, M., Citterio, E., van Lohuizen, M., and Ganesan, S. (2011) BMI1 is recruited to DNA breaks and contributes to DNA damage-induced H2A ubiquitination and repair. *Mol. Cell. Biol.* **31,** 1972–1982
20. Jacobs, J. J., Kieboom, K., Marino, S., DePinho, R. A., and van Lohuizen, M. (1999) The oncogene and Polycomb-group gene *bmi-1* regulates cell proliferation and senescence through the ink4a locus. *Nature* **397,** 164–168
21. Sauvageau, M., and Sauvageau, G. (2008) Polycomb group genes: keeping stem cell activity in balance. *PLoS Biol.* **6,** e113
22. Schwartz, Y. B., and Pirrotta, V. (2008) Polycomb complexes and epigenetic states. *Curr. Opin. Cell Biol.* **20,** 266–273
23. Nakayama, T., and Yamashita, M. (2009) Critical role of the Polycomb and Trithorax complexes in the maintenance of CD4 T cell memory. *Semin. Immunol.* **21,** 78–83
24. Camahort, R., and Cowan, C. A. (2012) Cbx proteins help ESCs walk the line between self-renewal and differentiation. *Cell Stem Cell* **10,** 4–6
25. Morey, L., Pascual, G., Cozzuto, L., Roma, G., Wutz, A., Benitah, S. A., and Di Croce, L. (2012) Nonoverlapping functions of the Polycomb group Cbx family of proteins in embryonic stem cells. *Cell Stem Cell* **10,** 47–62
26. O'Loghlen, A., Muñoz-Cabello, A. M., Gaspar-Maia, A., Wu, H. A., Banito, A., Kunowska, N., Racek, T., Pemberton, H. N., Beolchi, P., Lavial, F., Masui, O., Vermeulen, M., Carroll, T., Graumann, J., Heard, E., *et al.* (2012) MicroRNA regulation of Cbx7 mediates a switch of Polycomb orthologs during ESC differentiation. *Cell Stem Cell* **10,** 33–46
27. Reliene, R., Bishop, A. J., and Schiestl, R. H. (2007) Involvement of homologous recombination in carcinogenesis. *Adv. Genet.* **58,** 67–87
28. Ringrose, L., and Paro, R. (2004) Epigenetic regulation of cellular memory by the Polycomb and Trithorax group proteins. *Annu. Rev. Genet.* **38,** 413–443
29. Wang, H., Wang, L., Erdjument-Bromage, H., Vidal, M., Tempst, P., Jones, R. S., and Zhang, Y. (2004) Role of histone H2A ubiquitination in Polycomb silencing. *Nature* **431,** 873–7878
30. Schuettengruber, B., Chourrout, D., Vervoort, M., Leblanc, B., and Cavalli, G. (2007) Genome regulation by polycomb and trithorax proteins. *Cell* **128,** 735–745
31. Köhler, C., and Villar, C. B. (2008) Programming of gene expression by Polycomb group proteins. *Trends Cell Biol.* **18,** 236–243
32. Paro, R., and Hogness, D. S. (1991) The Polycomb protein shares a homologous domain with a heterochromatin-associated protein of *Drosophila*. *Proc. Natl. Acad. Sci. U.S.A.* **88,** 263–267
33. Chou, D. M., Adamson, B., Dephoure, N. E., Tan, X., Nottke, A. C., Hurov, K. E., Gygi, S. P., Colaiácovo, M. P., and Elledge, S. J. (2010) A chromatin localization screen reveals poly (ADP ribose)-regulated recruitment of the repressive polycomb and NuRD complexes to sites of DNA damage. *Proc. Natl. Acad. Sci. U.S.A.* **107,** 18475–18480
34. Jones, G. D., Ward, J. F., Limoli, C. L., Moyer, D. J., and Aguilera, J. A. (1995) Mechanisms of radiosensitization in iododeoxyuridine-substituted cells. *Int. J. Radiat. Biol.* **67,** 647–653
35. Senthilkumar, R., and Mishra, R. K. (2009) Novel motifs distinguish multiple homologues of Polycomb in vertebrates: expansion and diversification of the epigenetic toolkit. *BMC Genomics* **10,** 549
36. Hemenway, C. S., de Erkenez, A. C., and Gould, G. C. (2001) The polycomb protein MPc3 interacts with AF9, an MLL fusion partner in t(9;11)(p22;q23) acute leukemias. *Oncogene* **20,** 3798–3805
37. Miranda, T. B., Cortez, C. C., Yoo, C. B., Liang, G., Abe, M., Kelly, T. K., Marquez, V. E., and Jones, P. A. (2009) DZNep is a global histone methylation inhibitor that reactivates developmental genes not silenced by DNA methylation. *Mol. Cancer Ther.* **8,** 1579–1588
38. McCabe, M. T., Ott, H. M., Ganji, G., Korenchuk, S., Thompson, C., Van Aller, G. S., Liu, Y., Graves, A. P., Della Pietra, A., 3rd, Diaz, E., LaFrance, L. V., Mellinger, M., Duquenne, C., Tian, X., Kruger, R. G., *et al.* (2012) EZH2 inhibition as a therapeutic strategy for lymphoma with EZH2-activating mutations. *Nature* **492,** 108–112
39. Bárdos, J. I., Saurin, A. J., Tissot, C., Duprez, E., and Freemont, P. S. (2000) HPC3 is a new human polycomb orthologue that interacts and associates with RING1 and Bmi1 and has transcriptional repression properties. *J. Biol. Chem.* **275,** 28785–28792
40. Moding, E. J., Kastan, M. B., and Kirsch, D. G. (2013) Strategies for optimizing the response of cancer and normal tissues to radiation. *Nat. Rev. Drug Discovery* **12,** 526–542
41. Dungrawala, H., Rose, K. L., Bhat, K. P., Mohni, K. N., Glick, G. G., Couch, F. B., and Cortez, D. (2015) The replication checkpoint prevents two types of fork collapse without regulating replisome stability. *Mol. Cell* **59,** 998–1010
42. Mortusewicz, O., Amé, J. C., Schreiber, V., and Leonhardt, H. (2007) Feedback-regulated poly(ADPribosyl)ation by PARP-1 is required for rapid response to DNA damage in living cells. *Nucleic Acids Res.* **35,** 7665–7675
43. Haince, J. F., McDonald, D., Rodrigue, A., Déry, U., Masson, J. Y., Hendzel, M. J., and Poirier, G. G. (2008) PARP1-dependent kinetics of recruitment of MRE11 and NBS1 proteins to multiple DNA damage sites. *J. Biol. Chem.* **283,** 1197–1208
44. Karras, G. I., Kustatscher, G., Buhecha, H. R., Allen, M. D., Pugieux, C., Sait, F., Bycroft, M., and Ladurner, A. G. (2005) The macro domain is an ADP-ribose, binding module. *EMBO J.* **24,** 1911–1920
45. Eustermann, S., Brockmann, C., Mehrotra, P. V., Yang, J. C., Loakes, D., West, S. C., Ahel, I., and Neuhaus, D. (2010) Solution structures of the two PBZ domains from human APLF and their interaction with poly(ADP-ribose). *Nat. Struct. Mol. Biol.* **17,** 241–243
46. Yan, K. P., Dollé, P., Mark, M., Lerouge, T., Wendling, O., Chambon, P., and Losson, R. (2004) Molecular cloning, genomic structure, and expression analysis of the mouse transcriptional intermediary factor 1γ gene. *Gene* **334,** 3–13
47. Kulkarni, A., Oza, J., Yao, M., Sohail, H., Ginjala, V., Tomas-Loba, A., Horejsi, Z., Tan, A. R., Boulton, S. J., and Ganesan, S. (2013) Tripartite Motif-containing 33 (TRIM33) Protein Functions in the Poly(ADP-ribose) Polymerase (PARP)-dependent DNA Damage Response through Interaction with Amplified in Liver Cancer 1 (ALC1) Protein. *J. Biol. Chem.* **288,** 32357–32369
48. Jasin, M. (1996) Genetic manipulation of genomes with rare-cutting endonucleases. *Trends Genet.* **12,** 224–228
49. Xia, B., Sheng, Q., Nakanishi, K., Ohashi, A., Wu, J., Christ, N., Liu, X., Jasin, M., Couch, F. J., and Livingston, D. M. (2006) Control of BRCA2 cellular and clinical functions by a nuclear partner, PALB2. *Mol. Cell* **22,** 719–729
50. Bennardo, N., Cheng, A., Huang, N., and Stark, J. M. (2008) Alternative-NHEJ is a mechanistically distinct pathway of mammalian chromosome break repair. *PLoS Genet.* **4,** e1000110
51. House, N. C., Koch, M. R., and Freudenreich, C. H. (2014) Chromatin modifications and DNA repair: beyond double-strand breaks. *Front. Genet.* **5,** 296
52. Facchino, S., Abdouh, M., Chatoo, W., and Bernier, G. (2010) BMI1 confers radioresistance to normal and cancerous neural stem cells through recruitment of the DNA damage response machinery. *J. Neurosci.* **30,** 10096–10111
53. Ismail, I. H., Andrin, C., McDonald, D., and Hendzel, M. J. (2010) BMI1-mediated histone ubiquitylation promotes DNA double-strand break repair. *J. Cell Biol.* **191,** 45–60
54. Bernstein, E., Duncan, E. M., Masui, O., Gil, J., Heard, E., and Allis, C. D. (2006) Mouse polycomb proteins bind differentially to methylated histone H3 and RNA and are enriched in facultative heterochromatin. *Mol. Cell. Biol.* **26,** 2560–2569
55. Kaustov, L., Ouyang, H., Amaya, M., Lemak, A., Nady, N., Duan, S., Wasney, G. A., Li, Z., Vedadi, M., Schapira, M., Min, J., and Arrowsmith, C. H.

(2011) Recognition and specificity determinants of the human Cbx chromodomains. *J. Biol. Chem.* **286,** 521–529
56. Gao, Z., Zhang, J., Bonasio, R., Strino, F., Sawai, A., Parisi, F., Kluger, Y., and Reinberg, D. (2012) PCGF homologs, CBX proteins, and RYBP define functionally distinct PRC1 family complexes. *Mol. Cell* **45,** 344–356
57. Tavares, L., Dimitrova, E., Oxley, D., Webster, J., Poot, R., Demmers, J., Bezstarosti, K., Taylor, S., Ura, H., Koide, H., Wutz, A., Vidal, M., Elderkin, S., and Brockdorff, N. (2012) RYBP-PRC1 complexes mediate H2A ubiquitylation at polycomb target sites independently of PRC2 and H3K27me3. *Cell* **148,** 664–678
58. Shanbhag, N. M., Rafalska-Metcalf, I. U., Balane-Bolivar, C., Janicki, S. M., and Greenberg, R. A. (2010) ATM-dependent chromatin changes silence transcription in cis to DNA double-strand breaks. *Cell* **141,** 970–981
59. Vincenz, C., and Kerppola, T. K. (2008) Different polycomb group CBX family proteins associate with distinct regions of chromatin using nonhomologous protein sequences. *Proc. Natl. Acad. Sci. U.S.A.* **105,** 16572–16577
60. Xu, B., and Kastan, M. B. (2004) Analyzing cell cycle checkpoints after ionizing Radiation. *Methods Mol Biol.* **281,** 283–292
61. Franken, N. A., Rodermond, H. M., Stap, J., Haveman, J., and van Bree, C. (2006) Clonogenic assay of cells *in vitro*. *Nat. Protoc.* **1,** 2315–2319
62. Nakatani, Y., and Ogryzko, V. (2003) Immunoaffinity purification of mammalian protein complexes. *Methods Enzymol.* **370,** 430–444